CELEBRATING 5 YEARS

ACS OMEGA

pubs.acs.org/acsomega Volume 5, Issue 8 March 3, 2020

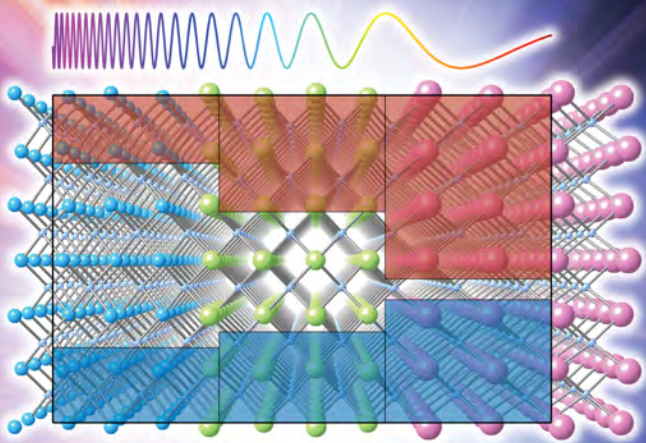

ACS Publications
Most Trusted. Most Cited. Most Read.

www.acs.org

ACS OMEGA

http://pubs.acs.org/journal/acsodf

Article

Band Alignments of Ternary Wurtzite and Zincblende III-Nitrides Investigated by Hybrid Density Functional Theory

Yi-Chia Tsai and Can Bayram*

Cite This: *ACS Omega* 2020, 5, 3917−3923

Read Online

ACCESS | Metrics & More | Article Recommendations | Supporting Information

ABSTRACT: Band gaps and electron affinities of binary and ternary, wurtzite (wz-) and zincblende (zb-) III-nitrides are investigated using a unified hybrid density functional theory, and band offsets between wz- and zb- alloys are calculated using Anderson's electron affinity model. A conduction (and valence) band offset of 1.85 (0.89) eV has been calculated for zb-GaN/InN heterojunctions, which is 0.25 eV larger (and 0.26 eV smaller) than that of the wz- counterpart. Such polarization-free zb-GaN/InGaN/GaN quantum well structures with large conduction band offsets have the potential to suppress electron leakage current and quantum-confined Stark effects (QCSEs). Contrarily, the conduction (and valence) band offset of zb-AlN/GaN heterojunctions is calculated to be 1.32 (0.43) eV, which is 1.15 eV smaller (and 0.13 eV larger) than that of the wz- case. The significant reduction in zb-AlN/GaN band offsets is ascribed to the smaller and indirect band gap of zb-AlN—the direct-to-indirect crossover point in zb-$Al_XGa_{1-X}N$ is when $X \sim 65\%$. The small band gap of the zb-AlN barrier and the small conduction band offsets imply that electrons can be injected into zb-AlN/GaN/AlN quantum well heterostructures with small bias and less energy loss when captured by the quantum wells, respectively, i.e., loss as heat is reduced. The band gap of ternary III-nitrides does not linearly depend on alloy compositions, implying a nonlinear dependence of band offsets on compositions. As a result, the large bowing of the conduction band offset is identified and ascribed to the cation-like behavior of the conduction band minimum, while the linear dependence of the valence band offset on compositions is attributed to the anion-like character of the valence band maximum.

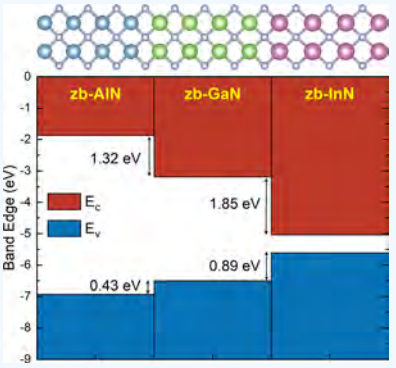

I. INTRODUCTION

III-nitrides (i.e., $Al_XGa_YIn_{(1-X-Y)}N$) have been instrumental in enabling ultraviolet and blue[1] light-emitting diodes (LEDs), high-frequency high-electron-mobility transistors (HEMTs),[2] and negative electron affinity photocathodes.[3] These devices rely on quantum structures[4] or buffer layers[3] composed of heterointerfaces. For instance, blue LEDs utilize GaN/InGaN/GaN quantum well heterostructures to increase the electron−hole spatial overlap for high emission efficiency, and HEMTs utilize AlGaN/GaN heterojunctions to form a two-dimensional electron gas channel for high-speed transport. These devices utilize the conventional wurtzite (wz-) phase of the III-nitrides that comes with challenges.[2] For instance, extending the LED spectrum from blue to green for the use of green LEDs in white light generation has been challenging as inherent spontaneous and piezoelectric polarization in wz- III-nitrides cause the electron−hole spatial separation in quantum wells (i.e., quantum-confined Stark effect (QCSE)), limiting the radiative efficiency. On the electronics side, the inherent spontaneous and piezoelectric polarization in wz- III-nitrides cause HEMTs to be normally on at all times, creating safety concerns in power electronics applications.[2] Zincblende (zb-) III-nitrides offer a solution to overcome these challenges as they are free of both spontaneous and piezoelectric polarization (in the ⟨001⟩ growth direction) thanks to the centrosymmetric crystal structure while having similar benefits.

zb- III-nitrides are realized traditionally via (i) direct deposition on zb substrates (e.g., GaAs,[5] 3C−SiC,[6] Si(100),[7] and MgO[8]) and (ii) transforming the wz- phase into a zb- one (ii.a) by impurity incorporation (such as Ga[8])[9] or (ii.b) by growth on *V*-[10−12] or *U*-grooved[13−15] patterned silicon substrates. Benefiting from this emerging material system is only possible through theoretically investigating the electronic properties. Particularly, band gaps, effective masses, and band offsets are needed to model the carrier dynamics in quantum structures.

We have recently reported analytical equations on band gaps and effective masses of wz- and zb- III-nitrides.[16] Although band alignments between wz-AlN, GaN, and InN have been reported experimentally,[17] band alignments between zb- III-nitrides remain vague. For instance, the reported valence band offsets of the unstrained zb-AlN/GaN interface range from 0.25 to 1.00 eV.[17] The variance in the reported band offset values is due to the choices of (i) approaches used to construct

Received: October 9, 2019
Accepted: January 20, 2020
Published: January 30, 2020

https://dx.doi.org/10.1021/acsomega.9b03353
ACS Omega 2020, 5, 3917−3923

the band structures (such as the hybrid density functional theory, the $k\cdot p$ perturbation theory, and the tight-binding model) and (ii) energy references (such as the vacuum level, average electrostatic potentials, charge neutrality levels, and branch-point energies).[18]

It is important to note that band alignments procured without the impact of strain are known as natural or unstrained band alignments, which are essential to determine the band alignments under a certain strain condition by incorporating deformation potentials.[19] In this work, a unified hybrid functional is introduced to determine band gaps and electron affinities of unstrained binary and ternary, wz- and zb- III-nitrides. The advantage of using the unified approach is that method accuracy is verified by the reported data on wz- III-nitrides, which enables calculating the electronic properties of zb- III-nitrides with high reliability. Electron affinities are calculated based on nonpolar wz- $(10\bar{1}0)$ and zb- (110) planes because earlier works show that interface orientations of (100), (110), and (111) have minor impacts on valence band offsets.[20] Band alignments of binary and ternary, wz- and zb- III-nitrides are derived from band gaps and electron affinities using Anderson's electron affinity model.[21]

II. RESULTS AND DISCUSSION

Figure 1a shows the electron affinity of binary and ternary III-nitrides. The x-axis labels the alloys ranging from InN and

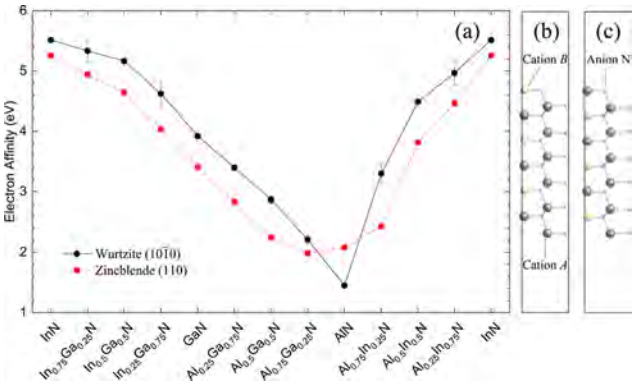

Figure 1. (a) Electron affinities of III-nitrides on the wz- $(10\bar{1}0)$ and zb- (110) planes. (b) Type-I and (c) type-II slabs for wz- III-nitrides with 25 or 75% alloying.

GaN to AlN, while the y-axis is the electron affinity. The black solid line and red dashed line indicate the $(10\bar{1}0)$ facet of wz-alloys and the (110) facet of zb- alloys, respectively. Qualitatively, the electron affinity of III-nitrides on the wz- $(10\bar{1}0)$ and zb- (110) facets has the analogous composition-dependent relation, which reaches the maximum at InN regardless of wz- and zb- crystals and decreases with respect to the increasing mole fraction of Al and Ga. The electron affinity of the wz- alloys reaches the minimum at AlN, while the electron affinity of the zb- alloys reaches the minimum around $Al_{0.75}Ga_{0.25}N$ because the conduction band minimum shifts from Γ- to X-valley, which will be explained later in light of the band alignments. Quantitatively, the electron affinity of 3.92 eV is obtained on the $(10\bar{1}0)$ facet of wz-GaN, which agrees with 4.06 ± 0.07 eV measured on the same facet.[22] It is worth noting that the electron affinity of 2.6−3.8 eV had been widely reported on the polar (0001) facet of wz-GaN.[23,24] The reduction of the electron affinity is attributed to the presence of surface adsorption and surface polarity. For instance, the electron affinities of Ga- and N-polar GaN surfaces have been reported to be 3.8 and 3.3 eV, respectively.[23] Experiments and recent generalized gradient approximation (GGA)-based simulations reveal that the electron concentration accumulated around the Ga- and N-dangling bonds at the GaN surface is too low to screen the spontaneous polarization-induced electric field. Consequently, the spontaneous polarization-induced electric field causes an upward surface band bending and leads to the reduction of electron affinity.[23,25] The calculated electron affinity of wz-AlN is 1.45 eV, which falls within the experimental values ranging from 0.25 ± 0.3 to 1.9 eV.[26,27] Notably, the large uncertainty is ascribed to the chemically active surface of AlN that is vulnerable to oxygen contamination. For the electron affinity of wz-InN, the measured range of 5.5−5.8 eV is deducted by the conduction band offset of the wz-GaN/InN heterojunction and the electron affinity of wz-GaN,[28] which are consistent with the theoretical values of 5.3 (In-polar c-plane)−5.8 (m-plane) eV using the GW calculation.[29] Our Heyd−Scuseria−Ernzerhof (HSE06) approach procures 5.51 eV for the electron affinity of wz-InN, which is in agreement with the experiments and the more advanced theory.

The electron affinity is sensitive to the atomic arrangement on the surface. wz- crystal structure has two distinct point bases; therefore, the unit cell used to build m-plane slabs involves two asymmetric cation−anion bonds. Since the slabs are generated by repeating the unit cell along the z-axis, two distinct cation bases lead to different surface stoichiometries for ternary wz- III-nitrides. If two different types of cations are involved in the slab, one type of the cations can lie either on the surface layer (type-I cation arrangement) or one atomic layer below the surface layer (type-II cation arrangement), as shown in Figure 1b,c, respectively. The asymmetric cation arrangements in the slab lead to different electron distributions, electrostatic potentials, and dipole moments, which render the surface band bending and the diminution of electron affinity.[25,30] Consequently, each ternary wz- III-nitride with 25 and 75% alloying ends in two distinct electron affinities depending on the surface stoichiometry represented by the error bars in Figure 1. For example, the electron affinities of wz-$In_{0.25}Ga_{0.75}N$ are 5.52 (surface terminates with an In−N bond) and 5.14 eV (surface terminates with a Ga−N bond). Table 1 tabulates the magnitude of the electron affinity and estimated dipole moments for the type-I and type-II cation arrangements. It proves that two different dipole moments are induced by the asymmetric surface stoichiometries. The amplitude of the electron affinity variation is small when the dipole moments are weak. The variation of the electron affinity directly contributes to the variation of band alignments.

Table 1. Electron Affinities and Estimated Dipole Moments of 25- and 75%-Alloying wz- III-Nitrides for Type-I and Type-II Cation Arrangements

alloy	electron affinity (eV)	dipole moment (type-I) (D)	dipole moment (type-II) (D)
$Al_{0.25}Ga_{0.75}N$	3.396 ± 0.048	0.084	0.018
$Al_{0.75}Ga_{0.25}N$	2.212 ± 0.065	0.095	0.036
$Al_{0.25}In_{0.75}N$	4.967 ± 0.203	0.399	0.351
$Al_{0.75}In_{0.25}N$	3.300 ± 0.167	0.430	0.269
$In_{0.25}Ga_{0.75}N$	4.624 ± 0.225	0.421	0.182
$In_{0.75}Ga_{0.25}N$	5.334 ± 0.191	0.273	0.663

https://dx.doi.org/10.1021/acsomega.9b03353
ACS Omega 2020, 5, 3917−3923

Therefore, the average value of electron affinities is exploited for band alignments, as shown in Figure 2.

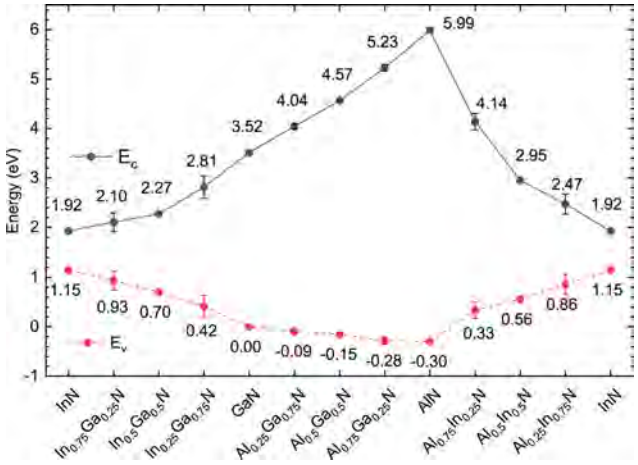

Figure 2. Conduction and valence band edges of binary and ternary wz- III-nitrides. The energies are shifted relative to the valence band maximum of wz-GaN.

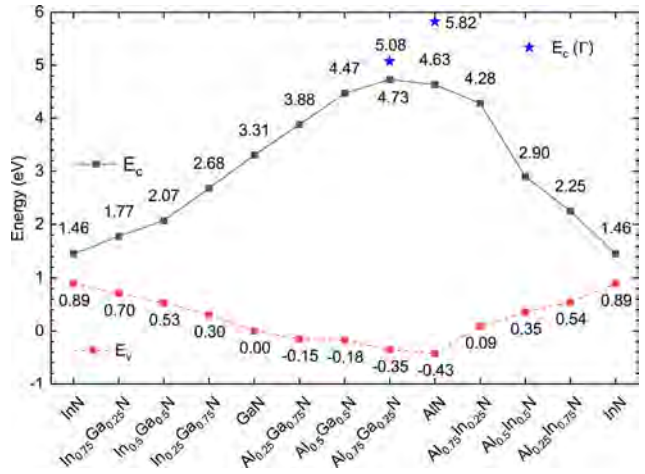

Figure 3. Conduction and valence band edges of binary and ternary zb- III-nitrides. The energies are shifted relative to the valence band maximum of zb-GaN. Two blue-star symbols indicate the conduction band edge at Γ-valley for indirect-gap alloys.

According to Anderson's electron affinity model, the band diagram of III-nitrides can be aligned with respect to the vacuum energy using the electron affinity and the band gap obtained from the density functional theory (DFT) calculations. Figure 2 summarizes the conduction (E_c) and valence (E_v) band edges of wz-InGaN, AlGaN, and AlInN indicated by the black solid line and red dashed line, respectively. Instead of using the vacuum energy as a reference level, the band edges are shifted relative to the valence band edge of wz-GaN for convenience. The conduction and valence band offsets between arbitrary two materials can be determined by the difference of E_c and E_v, respectively. As a result, the wz- alloys exhibit type-I band alignments, where the conduction (and valence) band offsets of wz-GaN/InN, wz-AlN/GaN, and wz-AlN/InN heterojunctions are 1.60 (1.15), 2.47 (0.30), and 4.07 (1.45) eV, leading to the ratios of conduction band offsets to band-gap differences of 0.58, 0.89, and 0.74, respectively. Before further exploration, it is important to validate the accuracy of the methodology through experimental measurements. To begin with, the valence band offset of 1.05 ± 0.25 eV has been probed experimentally for wz-GaN/InN heterojunctions,[31] which is in agreement with our simulation result of 1.15 eV. On the other hand, the calculated valence band offset of the wz-AlN/GaN heterostructure (0.3 eV) is consistent with the X-ray photoemission spectroscopy measurement of 0.3 ± 0.1 eV,[32] while, for wz-AlN/InN heterostructures, the calculated valence band offset of 1.45 eV agrees with the X-ray photoemission spectroscopy measurement of 1.4 ± 0.1 eV.[33] Notably, the deviation between the experiment and simulation and the uncertainty in experiments are ascribed to the variation of defectivity, strain, stoichiometry, surface polarity, and the chemical potency of reference core levels. Based on the validated methodology, the band alignments of zb- III-nitrides are calculated. Figure 3 demonstrates the conduction (black solid line) and valence (red dashed line) band edges of binary and ternary zb- III-nitrides relative to the valence band edge of zb-GaN. The blue-star symbols indicate the conduction band edge at Γ-valley for indirect-gap alloys. The direct-to-indirect crossover point of zb-$Al_{0.65}Ga_{0.35}N$ is interpolated by zb-$Al_{0.50}Ga_{0.50}N$ and zb-$Al_{0.75}Ga_{0.25}N$ when the conduction band minimum at Γ-valley has the same energy as that of X-valley. The crossover point is close to zb-$Al_{0.70}Ga_{0.30}N$ derived from the local density approximation (LDA-1/2) approach.[16] Similar to the wz-heterojunctions, type-I band alignments are observed among the zb- III-nitrides, where the conduction (and valence) band offsets of zb-GaN/InN, zb-AlN/GaN, and zb-AlN/InN heterojunctions are 1.85 (0.89), 1.32 (0.43), and 3.17 (1.32) eV, leading to the ratios of conduction band offsets to band-gap differences of 0.68, 0.75, and 0.71, respectively. Since the research in zb- III-nitrides is still in early stages, only the experimental band offsets of the zb-AlN/GaN heterojunction are available for validation. The conduction and valence band offsets of the zb-AlN/GaN heterojunction obtained from simulations are in agreement with the conduction and valence band offsets of 1.4 ± 0.1 and 0.5 ± 0.1 eV measured from inter-sub-band transition energies, where the ratio of the conduction band offset to the band-gap difference is 0.74 ± 0.05.[34] A constant mixing parameter of 0.25 had been reported to study the band gap of zb-AlN and zb-GaN and the band offsets of the zb-AlN/GaN heterojunction.[34] Consequently, the constant mixing parameter of 0.25 significantly underestimates the band gap of zb-AlN and zb-GaN by 0.74 and 0.38 eV, respectively, while the conduction and valence band offsets are 1.22 and 0.42 eV, which are 0.10 and 0.01 eV smaller than our results obtained using dynamic mixing parameters. The larger difference in the conduction band offset can be majorly attributed to the inaccurate band gaps and band-gap difference, whereas the consistent valence band offset implies a weak dependence on the mixing parameter. The previous study improves the accuracy of band gaps through the computationally expensive GW calculation; however, in this study, the dynamic mixing parameters are adopted for the same purpose. As a result, the conduction band offset reported after the GW correction is 1.31 eV, which is consistent with our results. Therefore, the main benefit of using dynamic mixing parameters is to improve the overall reliability and accuracy of band gaps, band-gap difference, and conduction band offset without using computationally

https://dx.doi.org/10.1021/acsomega.9b03353
ACS Omega 2020, 5, 3917−3923

Table 2. Conduction (ΔE_c) and Valence (ΔE_v) Band Offsets of Binary III-Nitrides for wz- and zb- Crystal Structures[a]

heterojunction	ΔE_c (eV)	ΔE_c^{exp} (eV)	ΔE_v (eV)	ΔE_v^{exp} (eV)	$\frac{\Delta E_c}{\Delta E_c + \Delta E_v}$	refs
wz-GaN/InN	1.60	1.65 ± 0.25	1.15	1.05 ± 0.25	0.58	31
wz-AlN/GaN	2.47	2.50 ± 0.10	0.30	0.30 ± 0.10	0.89	32
wz-AlN/InN	4.07	4.10 ± 0.10	1.45	1.40 ± 0.10	0.74	33
zb-GaN/InN	1.85		0.89		0.68	
zb-AlN/GaN	1.32	1.40 ± 0.10	0.43	0.50 ± 0.10	0.75	34
zb-AlN/InN	3.17		1.32		0.71	

[a]The ratios of conduction band offsets to band-gap differences are listed. The experimental conduction band offsets (ΔE_c^{exp}) are derived by assuming that the band gaps of wz-AlN, wz-GaN, wz-InN, zb-AlN, and zb-GaN are 6.2, 3.4, 0.7, 5.3, and 3.3 eV, respectively.

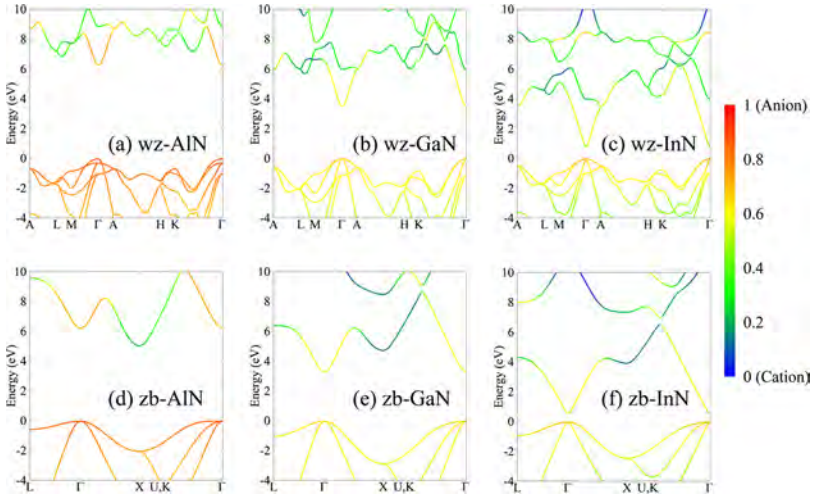

Figure 4. Element-projected electronic structure of (a) wz-AlN, (b) wz-GaN, (c) wz-InN, (d) zb-AlN, (e) zb-GaN, and (f) zb-InN. The red−light green colormap indicates an anion-like character, while the light green−blue colormap represents cation-like behavior.

expensive approaches. In short, the band offsets of binary wz- and zb- alloys are tabulated in Table 2.

The determination of band alignments in ternary III-nitrides is more complicated since it depends on the surface stoichiometry, as discussed in Figure 1, and the band-edge physics. The element-projected electronic structure of binary wz- and zb- III-nitrides is calculated to study the band-edge physics, as shown in Figure 4. The red−light green colormap indicates anion-like behavior, while the light green−blue colormap implies cation-like behavior. From observation in Figures 2 and 3, the valence band edge of ternary alloys can be linearly interpolated, though with a slight upward bowing for AlInN and InGaN. This is because the valence band maximum of AlN, GaN, and InN is composed mainly of anion orbital states regardless of wz- or zb- crystals. The anion-like character makes the valence band edge less sensitive to group-III alloying, which leads to the small bowing of valence band offsets. The slight upward bowing on the valence band edges of AlInN and InGaN can be ascribed to the energy shift of the valence band maximum with respect to the average energy of the top three valence bands at Γ-valley.[35] On the contrary, the conduction band edge of ternary alloys, except AlGaN, exhibits large bowing, which dominantly contributes to the band-gap bowing in both wz- and zb- crystals. Revealed by the element-projected electronic structure of wz-AlN, GaN, and InN, the conduction band minimum of wz-AlN at Γ-valley retains anion-like behavior; however, it dwindles as the increasing mole fraction of Ga and turns into a cation-like character in wz-InN. The anion-like conduction band edges in wz-AlGaN explain the relatively small bowing, whereas the cation-like conduction band edges in wz-AlInN and InGaN account for the large bowing. Likewise, the conduction band minima of zb-AlN, GaN, and InN at Γ-valley have the same anion-to-cation transition. Hence, the large bowing in the conduction band edges of zb-AlInN and InGaN is consistent with that of the wz-counterparts. A small bowing in the conduction band edges of zb-AlGaN is observed for zb-GaN, $Al_{0.25}Ga_{0.75}N$, and $Al_{0.5}Ga_{0.5}N$, but not for zb-$Al_{0.75}Ga_{0.25}N$ and AlN because the conduction band minimum of zb-$Al_{0.75}Ga_{0.25}N$ and AlN shifts from Γ-valley to X-valley. In comparison with the anion-like Γ-valley, X-valley has a strong cation-like character. Therefore, the conduction band minimum of zb-$Al_{0.75}Ga_{0.25}N$ and AlN at Γ-valley has the expected small bowing, but the conduction band minimum of zb-$Al_{0.75}Ga_{0.25}N$ and AlN at X-valley behaves oppositely.

By comparing the band offsets of the zb- alloys with those of the wz- alloys, the larger conduction band offset of the zb-GaN/InN heterojunction implies that LEDs made out of zb-GaN/InGaN quantum wells have a better electron capture rate, which suppresses electron leakage current. Likewise, the larger valence band offset of zb-AlN/GaN heterojunctions indicates a better hole capture rate in zb-AlGaN/GaN quantum wells. However, the conduction band offset of zb-AlN/GaN heterojunctions is significantly smaller than that of wz-AlN/GaN heterojunctions because zb-AlN has a small indirect band gap of 5.0−5.3 eV. Indeed, if we only consider the Γ-valley where the direct band gap occurs, the conduction band offsets of zb-AlGaN/GaN heterojunctions are identical to those of wz-AlGaN/GaN ones. For instance, the conduction band offsets of the zb-$Al_{0.25}Ga_{0.75}N$/GaN and zb-AlN/GaN

https://dx.doi.org/10.1021/acsomega.9b03353
ACS Omega 2020, 5, 3917−3923

heterojunctions are 0.57 and 2.51 eV in comparison with those of 0.52 and 2.47 eV in wz-$Al_{0.25}Ga_{0.75}N$/GaN and wz-AlN/GaN heterojunctions, respectively. The advantages of zb-AlN/GaN quantum wells over wz-AlN/GaN quantum wells are that the smaller band gap of the AlN barrier allows its devices to inject carriers with lower bias, whereas the smaller conduction band offset reduces energy loss when the electrons are captured by the quantum wells. Given the inherent polarization-free nature of zb-AlN/GaN quantum wells in the ⟨100⟩ direction, the electron capture of the shallow quantum wells can be increased using thicker quantum well designs with no QCSE. As a result, zb-AlN/GaN quantum wells are promising for energy-efficient emitters.

III. CONCLUSIONS

In summary, band gaps, electron affinities, and band alignments of wz- and zb- III-nitrides are calculated using a unified HSE06 hybrid functional, while the mixing parameters are calibrated from the experimental band gap of binary wz- III-nitrides. The band diagrams of III-nitrides are aligned using Anderson's electron affinity model. The conduction (and valence) band offsets of 1.60 (1.15) and 1.85 (0.89) eV are procured for the wz-GaN/InN and zb-GaN/InN heterojunctions. With polarization-free nature and large conduction band offsets, zb-GaN/InGaN/GaN quantum well heterostructures are promising to ameliorate electron capture and QCSE, leading to better radiative efficiency. On the other hand, the conduction (and valence) band offsets of 2.47 (0.30) and 1.32 (0.43) eV are obtained for the wz-AlN/GaN and zb-AlN/GaN heterojunctions. Devices made by the zb-AlN/GaN/AlN quantum well heterostructures are expected to be more energy-efficient than those of the wz- counterparts since the small band gap of the zb-AlN barrier and the small conduction band offsets indicate small bias and less energy loss when electrons are captured by the quantum wells, respectively. The band-gap bowing in wz- and zb- III-nitrides is dominantly contributed from the nonlinear dependence of the conduction band offset on compositions. We have found that the large bowing of the conduction band offsets is attributed to the cation-like conduction band minimum at Γ-valley, whereas the linear dependence of the valence band offsets is ascribed to the anion character of the valence band maximum.

IV. COMPUTATIONAL METHODS

Band gaps and electron affinities of wz- and zb- III-nitrides are calculated under the density functional theory (DFT) framework implemented in the Vienna ab initio simulation package (VASP).[36] Projector-augmented wave pseudopotentials with a cutoff kinetic energy of 500 eV are employed. Simulations are boiled down to bulk and slab calculations. In the bulk calculations, the conduction and valence band edges relative to the average electrostatic potential of the unit cell are determined. An eight-atom simple orthorhombic unit cell, which has the lattice vector $\vec{c}$ parallel to $(10\bar{1}0)$, is built for the wz- III-nitrides, while an eight-atom conventional cell is built for the zb- III-nitrides. A 6 × 4 × 4 and 5 × 5 × 5 Γ-centered Monkhorst–Pack set of *k*-points are sampled for the wz- and zb- unit cells, respectively. Local density approximation (LDA) and generalized gradient approximation (GGA) are well-known approaches to study the exchange–correlation interaction of ground-state electrons, but the excited states and band gap of III–V materials are commonly underestimated, which results in the inaccurate electron affinity and band offset overestimation.[37,38] Therefore, the HSE06 functional, which fixes band-gap underestimation by mixing the Hartree–Fock exchange energy with the Perdew–Becke–Ernzerhof (PBE) exchange energy, is adopted to describe the exchange–correlation interaction of III-nitrides. The optimal mixing parameters (α) of 0.341, 0.302, and 0.271 are found to reproduce the experimental band gaps of wz-AlN, GaN, and InN, respectively, while the optimal α of ternary III-nitrides is linearly interpolated by

$$\alpha = 0.341 \cdot x + 0.302 \cdot y + 0.271 \cdot (1 - x - y)$$

where x and y are the Al and Ga mole fractions, respectively. Details of finding the optimal α and accuracy of the linear interpolation are summarized in the supporting information (Figure S1). In the slab calculations, the vacuum energy is extracted using the macroscopic average of the electrostatic potential in the III-nitride thin film as a reference level. However, the thickness of the III-nitride thin film in the slab calculations should be large enough to recover the bulk-like electrostatic potential. According to the convergence tests (Figure S2), a 12-layer III-nitride thin film is large enough to recover the bulk-like electrostatic potential, which guarantees the accuracy of electron affinity. Therefore, 12-layer wz- and zb- slabs terminated with nonpolar $(10\bar{1}0)$ and (110) facets are generated from the preconverged bulk structures, respectively. An 18 Å vacuum space is reserved in the slabs. A 3 × 2 × 1 and 2 × 2 × 1 Γ-centered Monkhorst–Pack set of *k*-points are sampled for the wz- and zb- slabs, respectively. Each atom in the slabs is fully relaxed so that the interatomic force and energy difference are smaller than 0.01 eV $Å^{-1}$ and 10^{-6} eV, respectively. The macroscopic average of the electrostatic potential along the growth direction z of slabs is estimated by

$$\overline{\overline{V}}(z) = \frac{1}{lA}\int_{z-l/2}^{z+l/2}\int \mathrm{d}x\mathrm{d}y\mathrm{d}z'\Theta\left(\frac{l}{2} - |z - z'|\right)V(x, y, z')$$

where l, A, Θ, and V are the interlayer distance along the z-direction, the cross-sectional area of the slabs perpendicular to the z-direction, the Heaviside function, and the three-dimensional electrostatic potential of the slabs, respectively. The inner integral averages the electrostatic potential over the periodic directions so-called microscopic average, while the outer integral averages the periodic oscillation of the microscopic potential along the growth direction. Under the assumption that the average electrostatic potential of unit cells is identical to the macroscopic average of the electrostatic potential in the III-nitride thin film of the slabs, the electron affinity can be extracted by

$$\chi = (E_{vac} - \overline{\overline{V}}_{slab}) - (E_g + \mathrm{VBM} - \overline{\overline{V}}_{bulk})$$

where E_{vac} and $\overline{\overline{V}}_{slab}$ are the vacuum energy and the macroscopic average of the electrostatic potential in the III-nitride thin film procured from the slab calculations, while E_g, VBM, and $\overline{\overline{V}}_{bulk}$ are the band gap, the valence band maximum, and the average electrostatic potential of the unit cell obtained from the bulk calculations, respectively.

https://dx.doi.org/10.1021/acsomega.9b03353
ACS Omega 2020, 5, 3917−3923

■ ASSOCIATED CONTENT

Supporting Information

The Supporting Information is available free of charge at https://pubs.acs.org/doi/10.1021/acsomega.9b03353.

Figure S1 and Table S1 examine the accuracy of the hybrid density functional theory on the band gap of wz- and zb- binary III-nitrides calculated using different Hartree−Fock mixing parameters; and Figure S2 shows the electron affinity of wz-GaN as a function of thin film thickness (PDF)

■ AUTHOR INFORMATION

Corresponding Author

Can Bayram − *Department of Electrical and Computer Engineering, University of Illinois at Urbana-Champaign, Champaign, Illinois 61801, United States, Champaign, Illinois 61801, United States;* orcid.org/0000-0002-3987-1132; Email: cbayram@illinois.edu

Author

Yi-Chia Tsai − *Department of Electrical and Computer Engineering, University of Illinois at Urbana-Champaign, Champaign, Illinois 61801, United States, Champaign, Illinois 61801, United States;* orcid.org/0000-0003-2658-9397

Complete contact information is available at: https://pubs.acs.org/10.1021/acsomega.9b03353

Author Contributions

The manuscript was written through contributions of all authors. All authors have given approval to the final version of the manuscript.

Notes

The authors declare no competing financial interest.

■ ACKNOWLEDGMENTS

This work is supported by the National Science Foundation Faculty Early Career Development (CAREER) Program under award number NSF-ECCS-16-52871. The authors acknowledge the computational resources allocated by the Extreme Science and Engineering Discovery Environment (XSEDE) with Nos. TG-DMR180050 and TG-DMR180075.

■ REFERENCES

(1) Nakamura, S. *Shuji Nakamura - Nobel Lecture: Background Story of the Invention of Efficient Blue InGaN Light Emitting Diodes*, 2014.

(2) Morkoç, H. *Nitride Semiconductors and Devices*, Springer Series in Materials Science; Springer Berlin Heidelberg: Berlin, Heidelberg, 1999; Vol. 32.

(3) Machuca, F.; Liu, Z.; Maldonado, J. R.; Coyle, S. T.; Pianetta, P.; Pease, R. F. W. Negative Electron Affinity Group III-Nitride Photocathode Demonstrated as a High Performance Electron Source. *J. Vac. Sci. Technol., B* **2004**, *22*, 3565.

(4) Alferov, Z. I. The Double Heterostructure: Concept and Its Applications in Physics, Electronics and Technology. *Int. J. Mod. Phys. B* **2002**, *16*, 647.

(5) Yang, H.; Zheng, L. X.; Li, J. B.; Wang, X. J.; Xu, D. P.; Wang, Y. T.; Hu, X. W.; Han, P. D. Cubic-Phase GaN Light-Emitting Diodes. *Appl. Phys. Lett.* **1999**, *74*, 2498.

(6) Wei, C. H.; Xie, Z. Y.; Li, L. Y.; Yu, Q. M.; Edgar, J. H. MOCVD Growth of Cubic GaN on 3C-SiC Deposited on Si (100) Substrates. *J. Electron. Mater.* **2000**, *29*, 317.

(7) Goldys, E. M.; Godlewski, M.; Langer, R.; Barski, A.; Bergman, P.; Monemar, B. Analysis of the Red Optical Emission in Cubic GaN Grown by Molecular-Beam Epitaxy. *Phys. Rev. B* **1999**, *60*, 5464.

(8) Sanorpim, S.; Kuntharin, S.; Parinyataramas, J.; Yaguchi, H.; Iwahashi, Y.; Orihara, M.; Hijikata, Y.; Yoshida, S.; Ihm, J.; Cheong, H. High Cubic-Phase Purity InN on MgO (001) Using Cubic-Phase GaN as a Buffer Layer. *AIP Conf. Proc.* **2011**, 131−132.

(9) Dhara, S.; Datta, A.; Wu, C. T.; Lan, Z. H.; Chen, K. H.; Wang, Y. L.; Hsu, C. W.; Shen, C. H.; Chen, L. C.; Chen, C. C. Hexagonal-to-Cubic Phase Transformation in GaN Nanowires by Ga+ Implantation. *Appl. Phys. Lett.* **2004**, *84*, 5473.

(10) Cui, Y.; Lazorov, V. K.; Goetz, M. M.; Liu, H.; Robertson, D. P.; Gajdardziska-Josifovska, M.; Li, L. Cubic GaN Formation in Mn/GaN Multilayer Films Grown on 6H-SiC(0001). *Appl. Phys. Lett.* **2003**, *82*, 4666.

(11) Lee, S. C.; Pattada, B.; Hersee, S. D.; Jiang, Y.-B.; Brueck, S. R. Nanoscale Spatial Phase Modulation of GaN on a V-Grooved Si Substrate-Cubic Phase GaN on Si(001) for Monolithic Integration. *IEEE J. Quantum Electron.* **2005**, *41*, 596.

(12) Stark, C. J. M.; Detchprohm, T.; Lee, S. C.; Jiang, Y.-B.; Brueck, S. R. J.; Wetzel, C. Green Cubic GaInN/GaN Light-Emitting Diode on Microstructured Silicon (100). *Appl. Phys. Lett.* **2013**, *103*, No. 232107.

(13) Liu, R.; Schaller, R.; Chen, C. Q.; Bayram, C. High Internal Quantum Efficiency Ultraviolet Emission from Phase-Transition Cubic GaN Integrated on Nanopatterned Si(100). *ACS Photonics* **2018**, *5*, 955.

(14) Liu, R.; Bayram, C. Maximizing Cubic Phase Gallium Nitride Surface Coverage on Nano-Patterned Silicon (100). *Appl. Phys. Lett.* **2016**, *109*, No. 042103.

(15) Bayram, C.; Ott, J. A.; Shiu, K.-T.; Cheng, C.-W.; Zhu, Y.; Kim, J.; Razeghi, M.; Sadana, D. K. Cubic Phase GaN on Nano-Grooved Si (100) via Maskless Selective Area Epitaxy. *Adv. Funct. Mater.* **2014**, *24*, 4492.

(16) Tsai, Y. C.; Bayram, C. Structural and Electronic Properties of Hexagonal and Cubic Phase AlGaInN Alloys Investigated Using First Principles Calculations. *Sci. Rep.* **2019**, *9*, No. 6583.

(17) Vurgaftman, I.; Meyer, J. R. Band Parameters for Nitrogen-Containing Semiconductors. *J. Appl. Phys.* **2003**, *94*, 3675.

(18) Landmann, M.; Rauls, E.; Schmidt, W. G. Understanding Band Alignments in Semiconductor Heterostructures: Composition Dependence and Type-I-Type-II Transition of Natural Band Offsets in Nonpolar Zinc-Blende $Al_xGa_{1-x}N/Al_yGa_{1-y}N$ Composites. *Phys. Rev. B* **2017**, *95*, No. 155310.

(19) Van de Walle, C. G. Band Lineups and Deformation Potentials in the Model-Solid Theory. *Phys. Rev. B* **1989**, *39*, 1871.

(20) Binggeli, N.; Ferrara, P.; Baldereschi, A. Band-Offset Trends in Nitride Heterojunctions. *Phys. Rev. B* **2001**, *63*, No. 245306.

(21) Anderson, R. L. Germanium-Gallium Arsenide Heterojunctions [Letter to the Editor]. *IBM J. Res. Dev.* **1960**, *4*, 283.

(22) Portz, V.; Schnedler, M.; Eisele, H.; Dunin-Borkowski, R. E.; Ebert, P. Electron Affinity and Surface States of GaN M-Plane Facets: Implication for Electronic Self-Passivation. *Phys. Rev. B* **2018**, *97*, No. 115433.

(23) Lin, S.-C.; Kuo, C.-T.; Liu, X.; Liang, L.-Y.; Cheng, C.-H.; Lin, C.-H.; Tang, S.-J.; Chang, L.-Y.; Chen, C.-H.; Gwo, S. Experimental Determination of Electron Affinities for InN and GaN Polar Surfaces. *Appl. Phys. Express* **2012**, *5*, No. 031003.

(24) Strite, S. GaN, AlN, and InN: A Review. *J. Vac. Sci. Technol., B* **1992**, *10*, 1237.

(25) Krukowski, S.; Kempisty, P.; Strąk, P. Foundations of Ab Initio Simulations of Electric Charges and Fields at Semiconductor Surfaces within Slab Models. *J. Appl. Phys.* **2013**, *114*, No. 143705.

(26) Grabowski, S. P.; Schneider, M.; Nienhaus, H.; Mönch, W.; Dimitrov, R.; Ambacher, O.; Stutzmann, M. Electron Affinity of $Al_xGa_{1-x}N(0001)$ Surfaces. *Appl. Phys. Lett.* **2001**, *78*, 2503.

(27) Wu, C. I.; Kahn, A. Electronic States at Aluminum Nitride Surfaces. *Appl. Phys. Lett* **1999**, *74*, 546.

(28) Ager, J. W.; Miller, N. R. Taming Transport in InN. *Phys. Status Solidi A* **2012**, *209*, 83.
(29) Belabbes, A.; Furthmüller, J.; Bechstedt, F. Electronic Properties of Polar and Nonpolar InN Surfaces: A Quasiparticle Picture. *Phys. Rev. B* **2011**, *84*, No. 205304.
(30) Edmonds, M. T.; Pakes, C. I.; Mammadov, S.; Zhang, W.; Tadich, A.; Ristein, J.; Ley, L. Surface Band Bending and Electron Affinity as a Function of Hole Accumulation Density in Surface Conducting Diamond. *Appl. Phys. Lett.* **2011**, *98*, No. 102101.
(31) Martin, G.; Botchkarev, A.; Rockett, A.; Morkoç, H. Valence-band Discontinuities of Wurtzite GaN, AlN, and InN Heterojunctions Measured by X-ray Photoemission Spectroscopy. *Appl. Phys. Lett.* **1996**, *68*, 2541.
(32) Rizzi, A.; Lantier, R.; Monti, F.; Lüth, H.; Della Sala, F.; Di Carlo, A.; Lugli, P. AlN and GaN Epitaxial Heterojunctions on 6H-SiC(0001): Valence Band Offsets and Polarization Fields. *J. Vac. Sci. Technol., B* **1999**, *17*, 1674.
(33) Kuo, C. T.; Chang, K. K.; Shiu, H. W.; Liu, C. R.; Chang, L. Y.; Chen, C. H.; Gwo, S. Natural Band Alignments of InN/GaN/AlN Nanorod Heterojunctions. *Appl. Phys. Lett.* **2011**, *99*, No. 122101.
(34) Mietze, C.; Landmann, M.; Rauls, E.; Machhadani, H.; Sakr, S.; Tchernycheva, M.; Julien, F. H.; Schmidt, W. G.; Lischka, K.; As, D. J. Band Offsets in Cubic GaN/AlN Superlattices. *Phys. Rev. B* **2011**, *83*, No. 195301.
(35) Moses, P. G.; Miao, M.; Yan, Q.; Van de Walle, C. G. Hybrid Functional Investigations of Band Gaps and Band Alignments for AlN, GaN, InN, and InGaN. *J. Chem. Phys.* **2011**, *134*, No. 084703.
(36) Kresse, G.; Hafner, J. Ab Initio Molecular Dynamics for Liquid Metals. *Phys. Rev. B* **1993**, *47*, 558.
(37) Tran, F.; Blaha, P. Accurate Band Gaps of Semiconductors and Insulators with a Semilocal Exchange-Correlation Potential. *Phys. Rev. Lett.* **2009**, *102*, No. 226401.
(38) Mietze, C.; Landmann, M.; Rauls, E.; MacHhadani, H.; Sakr, S.; Tchernycheva, M.; Julien, F. H.; Schmidt, W. G.; Lischka, K.; As, D. J. Band Offsets in Cubic GaN/AlN Superlattices. *Phys. Rev. B* **2011**, *83*, No. 195301.

https://dx.doi.org/10.1021/acsomega.9b03353
ACS Omega 2020, 5, 3917−3923

Supporting Information

Band Alignments of Ternary Wurtzite and Zincblende III-Nitrides Investigated by Hybrid Density Functional Theory

Yi-Chia Tsai and Can Bayram*

Department of Electrical and Computer Engineering, University of Illinois at Urbana-Champaign, Champaign, Illinois, 61801, United States

Nick Holonyak, Jr Micro and Nanotechnology Laboratory, University of Illinois at Urbana-Champaign, Champaign, Illinois, 61801, United States

This pdf file includes:

*Innovative COmpound semiconductoR LABoratory (ICORLAB); Email: cbayram@illinois.edu; Webpage: icorlab.ece.illinois.edu; Phone: +1 (217) 300-0978; Fax: +1 (217) 244-6375

Accuracy of HSE06 Functional on the Band Gap of III-Nitrides

Conventional density-functional theory, (e.g. generalized gradient approximations (GGA), local-density approximations (LDA)) is able to retrieve the accurate ground-state properties. However, it commonly underestimates the band gaps of materials. HSE06 hybrid functional was proposed to improve the accuracy of band gap by mixing Hartree-Fock exact exchange energy with Perdew-Burke-Ernzerhof (PBE) functional. Different mixing parameters are benchmarked against experimental data for wurtzite (wz-) AlN, GaN, and InN. The first step is to try different mixing parameters from 0.25 to 0.35. It shows that the band gaps are linearly dependent on the mixing parameters. Therefore, the optimal mixing parameters of wz-AlN, GaN, and InN are calculated by linear interpolation using the experimental band gaps.[1] Using the optimal mixing parameters, the calculated band gaps of wz-AlN, GaN, and InN are consistent with the experimental band gaps as tabulated in Table S1. To ensure the consistency, the same optimal mixing parameters are used for its zincblende (zb-) counterparts. As the result, calculated band gaps of zb-AlN, GaN, and InN are in agreement with the experimentally-measured band gaps. To retain the accuracy for ternary III-nitrides, the optimal mixing parameter is linearly interpolated depending on the chemical compositions expressed as

$$\alpha = 0.341 \cdot x + 0.302 \cdot y + 0.271 \cdot (1 - x - y),$$

where x and y are the Al and Ga mole fractions, respectively. Given the better control of wz- crystal quality in experiment and the ample studies that have been accomplished, the experimental band gaps of wz- alloys are used to validate the accuracy of the interpolation. Figure S1 compares calculated band gaps of wz- (a) AlGaN, (b) AlInN, and (c) InGaN with experimental measurements.[2–7] Figure S1 shows that the mixing parameter interpolation for ternary alloys is able to procure the experimental band gaps.

Table S1. Band gap of wz- and zb- binary III-nitrides calculated using different Hartree-Fock mixing parameters (α) for HSE06 functional. The optimal mixing parameter (α_{opt}) for wz- alloys is obtained by linear interpolation; whereas, zb- alloys use the same α_{opt} as its wz- counterparts. The experimental band gaps are extracted from Ref. 1 unless noted otherwise.

Alloy	$E_g(\alpha = 0.25)$	$E_g(\alpha = 0.30)$	$E_g(\alpha = 0.35)$	α_{opt}	$E_g(\alpha = \alpha_{opt})$	E_g^{exp}
wz-AlN	5.672	6.002	6.340	0.341	6.284	6.250
wz-GaN	3.178	3.495	3.831	0.302	3.516	3.510
wz-InN	0.680	0.922	1.167	0.271	0.773	0.780
zb-AlN	4.578	4.841	5.110	0.341	5.060	5.040[8], 5.340
zb-GaN	2.977	3.291	3.619	0.302	3.307	3.299
zb-InN	0.476	0.731	0.956	0.271	0.564	0.560[9]

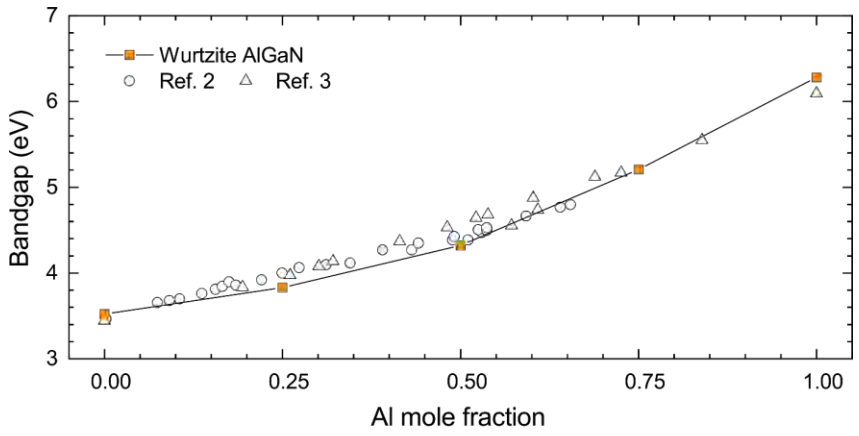

(a)

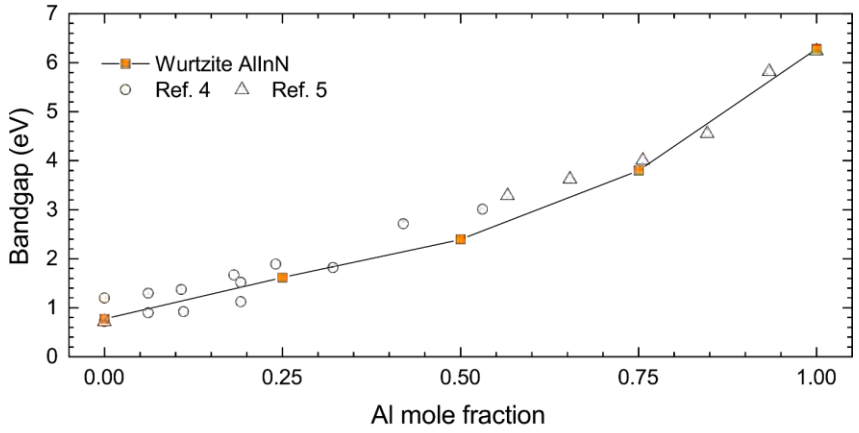

(b)

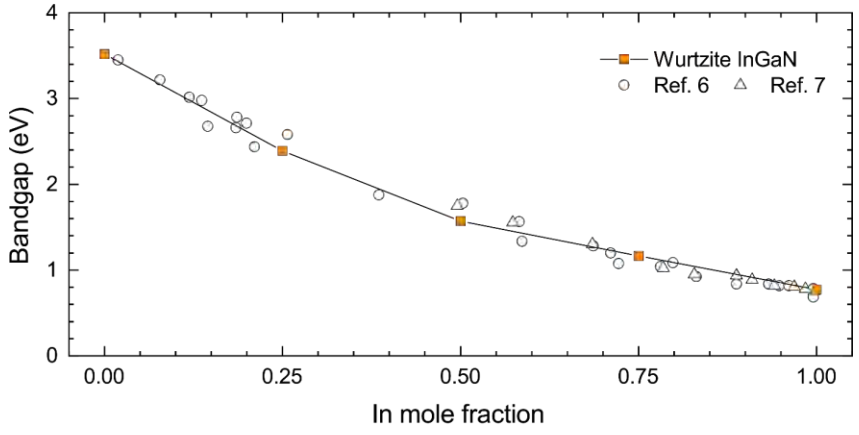

(c)

Figure S1. The calculated and experimental band gaps of wz- (a) AlGaN, (b) AlInN, and (c) InGaN.

Convergence Test of the Slab Thickness

The electron affinity of III-nitrides is obtained from two steps: bulk and slab calculations. In the bulk calculation, the conduction and valence band edges are retrieved using the average electrostatic potential of unit cells as a reference level. On the other hand, in the slab calculations, the vacuum energy relative to the macroscopic average of the electrostatic potential in III-nitrides thin film is calculated. By assuming the average of electrostatic potential in bulk and slab calculations are identical, the electron affinity can be derived by the definition:

$$\chi = \left(E_{vac} - \bar{\bar{V}}_{slab}\right) - \left(E_g + VBM - \bar{\bar{V}}_{bulk}\right),$$

where E_{vac} and $\bar{\bar{V}}_{slab}$ are the vacuum energy and the macroscopic average of electrostatic potential in the III-nitrides thin-film procured from the slab calculations; while, E_g, VBM, and $\bar{\bar{V}}_{bulk}$ are the band gap, the valence band maximum, and the average electrostatic potential of unit cells obtained from the bulk calculations, respectively. However, the thickness of III-nitrides thin film in slab calculations should be large enough to recover the bulk-like electrostatic potential, i.e. satisfy the assumption. A convergence test of electron affinity on the thickness of III-nitrides in slab calculations is performed. Figure S2 plots the electron affinity of wz-GaN as a function of the number layer of III-nitrides thin film. It shows that the electron affinity converges when the wz-GaN thin film is thicker than 8 atomic layers. For a higher accuracy and cost-effectiveness, 12-layer thin film is constructed for individual III-nitrides in slab calculations.

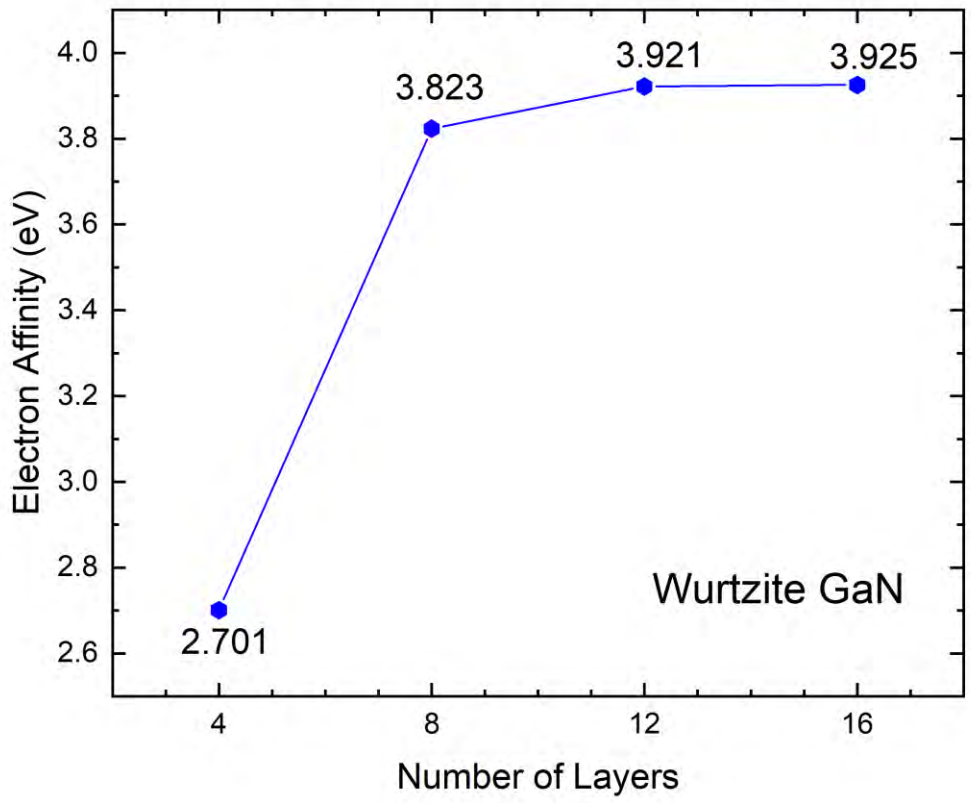

Figure S2. The electron affinity of wz-GaN as a function of thin film thickness.

REFERENCES

(1) Vurgaftman, I.; Meyer, J. R. Band Parameters for Nitrogen-Containing Semiconductors. *J. Appl. Phys.* **2003**, *94*, 3675.

(2) Leroux, M.; Dalmasso, S.; Natali, F.; Helin, S.; Touzi, C.; Laügt, S.; Passerel, M.; Omnes, F.; Semond, F.; Massies, J.; et al. Optical Characterization of $Al_xGa_{1-X}N$ Alloys ($x < 0.7$) Grown on Sapphire or Silicon. *Phys. status solidi* **2002**, *234*, 887.

(3) Paduano, Q. S.; Weyburne, D. W.; Bouthillette, L. O.; Wang, S.-Q.; Alexander, M. N. The Energy Band Gap of $Al_xGa_{1-x}N$. *Jpn. J. Appl. Phys.* **2002**, *41*, 1936.

(4) Naoi, H.; Fujiwara, K.; Takado, S.; Kurouchi, M.; Muto, D.; Araki, T.; Na, H.; Nanishi, Y. Growth of In-Rich $In_xAl_{1-x}N$ Films on (0001) Sapphire by RF-MBE and Their Properties. *J. Electron. Mater.* **2007**, *36*, 1313.

(5) Onuma, T.; Chichibu, S.; Uchinuma, Y.; Sota, T.; Yamaguchi, S.; Kamiyama, S.; Amano, H.; Akasaki, I. Recombination Dynamics of Localized Excitons in $Al_{1-x}In_xN$ Epitaxial

Films on GaN Templates Grown by Metalorganic Vapor Phase Epitaxy. *J. Appl. Phys.* **2003**, *94*, 2449.

(6) Franssen, G.; Gorczyca, I.; Suski, T.; Kamińska, A.; Pereiro, J.; Muñoz, E.; Iliopoulos, E.; Georgakilas, A.; Che, S. B.; Ishitani, Y.; et al. Bowing of the Band Gap Pressure Coefficient in $In_xGa_{1-x}N$ Alloys. *J. Appl. Phys.* **2008**, *103*, 033514.

(7) Wu, J.; Walukiewicz, W.; Yu, K. M.; Ager, J. W.; Haller, E. E.; Lu, H.; Schaff, W. J. Small Band Gap Bowing in $In_{1-X}Ga_xN$ Alloys. *Appl. Phys. Lett.* **2002**, *80*, 4741.

(8) Suzuki, T.; Yaguchi, H.; Okumura, H.; Ishida, Y.; Yoshida, S. Optical Constants of Cubic GaN, AlN, and AlGaN Alloys. *Jpn. J. Appl. Phys.* **2000**, *39*, L497.

(9) Schörmann, J.; As, D. J.; Lischka, K.; Schley, P.; Goldhahn, R.; Li, S. F.; Löffler, W.; Hetterich, M.; Kalt, H. Molecular Beam Epitaxy of Phase Pure Cubic InN. *Appl. Phys. Lett.* **2006**, *89*, 261903.